A NOVEL DESIGN OF MRI VISIBLE PROSTATE BIOPSY NEEDLE

by

Gökçe Kasacı

B.S., Bioengineering, Yıldız Technical University, 2012

Submitted to the Institute of Biomedical Engineering

in partial fulfillment of the requirements

for the degree of

Master of Science

in

Biomedical Engineering

Boğaziçi University

2017

A NOVEL DESIGN OF MRI VISIBLE PROSTATE BIOPSY NEEDLE

APPROVED BY:

Assist. Prof. Dr. Özgür Kocatürk   . . . .
(Thesis Advisor)

Prof. Dr. Cengizhan Öztürk   . . . .

Assoc. Prof. Dr. Erkan Kaplanoğlu   . . . .

DATE OF APPROVAL: 20 June 2017

ACKNOWLEDGEMENTS

Foremost, I would like to express my sincere thanks to my advisor Asst. Prof. Özgür Kocatürk for opportunities he has given me and for his continuous support, motivation and immense guidance throughout the time we worked together. I can openheartedly say that he is more than a supervisor to me. In addition, I express my appreciation to Prof. Dr. Cengizhan Öztürk and Assoc. Prof. Erkan Kaplanoğlu for having served on my committee. Their thoughtful questions and comments were valued greatly. I would also like to express my deepest thanks to Ahmet Turan Talaş for his extraordinary helps. Without his continuous support, the studies that are presented here could not possibly have been accomplished. I also thanks to Davut İbrahim Mahçiçek for his recommendations during the teamwork on this project.

I would like to send lots of love and thanks to Agah Karakuzu for his unlimited helps and every moment we shared with a cup of coffee, literature, music and many things that I cannot fit on this page.

Special thanks to Taylan Atakuru for his helps and friendship that were very valuable. Thanks to Günay Turan and Sinem Orbay for their sincere helps, but also for teaching me how important friendship is.

Thanks to Dr. Metin Vural and the American Hospital personnel for their kind helps.

I owe the sincere gratitude to my family, Hakan Kasacı, Tülin Kasacı and my lovely sister Sevim Kasacı for their unconditional love and supports in all conditions. I could not be who I am without them.

ACADEMIC ETHICS AND INTEGRITY STATEMENT

I, Gökçe Kasacı, hereby certify that I am aware of the Academic Ethics and Integrity Policy issued by the Council of Higher Education (YÖK) and I fully acknowledge all the consequences due to its violation by plagiarism or any other way.

Name :

Signature:

_____

_____

Date:

_____

ABSTRACT

A NOVEL DESIGN OF MRI VISIBLE PROSTATE BIOPSY NEEDLE

A reliable diagnosis is vital to apply the proper treatment for prostate cancer. Conventional prostate biopsy methods have limited accuracy for the diagnosis. Magnetic Resonance Imaging (MRI) provides superior anatomical images of the prostate, offering precise tumor targeting which in turn increases diagnostic yield. For that purpose, we aimed to develop a novel MRI compatible and visible prostate biopsy needle. The visible distal tip of the needle is expected to provide accurate placement while the proposed biopsy mechanism can reduce the bleeding and infection risk. The prostate biopsy needle has been designed using MRI compatible nitinol hypo tubes and fabricated using an Nd: YAG laser cutting system. Furthermore, the distal tip sharpness and force resistance of the three different needle designs were tested in vitro (silicon mold). According to results the needle with high walled biopsy groove was preferable. Equally spaced Iron Oxide (Fe_2O_3) nano-particle coatings were placed over the distal tip of the outer needle surface to enhance its visibility under real time MRI. The coating concentration and marker size were optimized using different MR sequences. MRI visibility experiments indicate that spin-echo acquisitions should be preferred over gradient-echo acquisitions and Fe_2O_3 coatings with moderate concentrations appear to be more suitable for the passive tracking of penetration depth. The biopsy needle handle also has been designed in Solidworks 2015 and generated using a rapid prototyping system. Finally, the in-vitro performance of the biopsy mechanism was carried out on fresh veal meat. Obtained samples indicate that Nd: YAG laser cutting can be successfully utilized in nitinol needle production and the biopsy handle design provided repeatable successful biopsy sample collections through in vitro trials.

Keywords: interventional MRI, prostate biopsy, biopsy needle, passive device visualization

ÖZET

MRG ALTINDA GÖRÜNTÜLENEBİLEN YENİ NESİL PROSTAT BİYOPSİ İĞNESİ

Prostat kanseri tedavisi için güvenilir bir tanı yöntemi oldukça önemlidir. Bilinen prostat biyopsi tanı yöntemlerinin doğruluğu sınırlıdır. Manyetik Rezonans Görüntüleme (MRG), prostatın daha detaylı ve daha kaliteli anatomik görüntülerini çıkardığı için tümörün daha kesin bir şekilde tespitini yapıp tanısal verimi arttırır. Yapmış olduğumuz projede bu amaç doğrultusunda, MRG uyumlu ve MRG altında görüntülenebilen prostat biyopsi iğnesi geliştirmeyi hedefledik. Önerilen biyopsi mekanizması kanama ve enfeksiyon riskini azaltırken, iğnenin görüntülenebilen uç kısmını tümörlü bölgeye doğru bir şekilde yerleştirmesi beklenir. Prostat biyopsi iğnesi MR uyumlu nitinol hipo tüpler kullanılarak tasarlanmış ve Nd: YAG lazer kesim sistemi kullanılarak üretilmiştir. Buna ek olarak, uç keskinliği ve biyopsi oyuğu farklılaştırılmış üç iğnenin kuvvet direnci laboratuvar ortamında test edilmiştir. Sonuçlar doğrultusunda, yüksek duvarlı biyopsi oyuğu olan iğnenin dayanımı daha fazla olduğu gözlemlendiğinden bu iğnenin tercih edilmesine karar verilmiştir. Dış iğne yüzeyinin uç kısmına eşit aralıklarla kaplanan demir oksit (Fe_2O_2) nano parçacıkların gerçek zamanlı MR görüntüsünde görünürlüğü arttırdığı görmek için kaplama yoğunlukları farklı MR dizileri kullanılarak optimize edilmiştir. MR görünürlük deneyleri, spin eko tabanlı görüntülerin gradyan eko tabanlı görüntülere göre tercih edileceği ve orta yoğunluklardaki Fe2O3 kaplamalarının penetrasyon derinliğinin pasif olarak izlenmesi için daha uygun olduğu görülmüştür. Biyopsi iğne tabancası da Solidworks 2015 kullanılarak tasarlanmış ve hızlı prototip sistemi kullanılarak üretilmiştir. Son olarak, biyopsi mekanizmasının laboratuvar ortamındaki performansı taze dana eti üzerinde gerçekleştirilip, elde edilen sonuçlar, Ng: YAG lazer kesme işleminin nitinol iğne üretiminde başarılı bir şekilde kullanılabileceğini ve biyopsi tutacağı tasarımının laboratuvar ortamındaki denemeler yoluyla tekrarlanabilir başarılı biyopsi numuneleri sağladığını göstermiştir.

Anahtar Sözcükler: Girişimsel MRG, prostat, biyopsi iğnesi, pasif cihaz görüntüleme

TABLE OF CONTENTS

LIST OF FIGURES

LIST OF TABLES

LIST OF SYMBOLS

C	Contrast
S_b	Signal from background
S_c	Signal from tracking device

LIST OF ABBREVIATIONS

ADC	Apparent Diffusion Coefficient
BPH	Benign Prostatic Hyperplasia
CT	Computed Tomography
CZ	Central Zone
DCE	Dynamic Contrast Enhanced Imaging
DRE	Digital Rectal Examination
EUM	Enhanced Ultrasound Modalities
FA	Fractional Anisotropy
FISP	Fast Imaging with Steady State Precession
GRE	Gradient Echo
HASTE	Half-Fourier Acquisition Single-Shot Turbo Spin-Echo
ID	Inner Diameter
IOMPs	Iron-Oxide Magnetic Nanoparticles
MD	Mean Diffusion
MRI	Magnetic Resonance Imaging
MRS	Magnetic Resonance Spectroscopy
Nd:YAG	YAG neodymium-doped Yttrium Aluminum Garnet
PCa	Prostate Cancer
PD	Projection Dephasing
PSA	Prostate Specific Antigen
PIRADS	Prostate Imaging Reporting and Data System
PET	Positron Emmision Tomography
PSA	Prostate Specific Antigen
PZ	Peripheral Zone
RF	Radio Frequency
SE	Spin Echo
SNR	Signal to Noise Ratio
T1w	T1 Weighted

T2w	T2 Weighted
TRUS	Transrectal Ultrasound
TSE	Turbo Spin Echo
TZ	Transitional Zone
OD	Outer Diameter
VIBE	Volumetric Interpolated Brain Examination
UV	Ultraviolet

1. INTRODUCTION

Prostate cancer (PCa) is one of the most common diseases among elderly adult men that causes mortality, requires accurate diagnosis and careful screening to get more positive results [1]. Mortality and morbidity rates are noteworthily high. The cause of the cancer is the uncontrolled cell growth. There are many different factors playing a role as its origin of genesis, including genetic make up, environmental conditions and precursor diseases etc. [2]. Irrespective of the origin of the PCa, early diagnosis is vital to cure the cancer before number of cancer cells increase and spread to the other organs of the body, called as metastasis. Especially when cancerous growth breaks through extracellular capsule of the prostate, the spreading is highly aggressive, that constitutes a high risk of metastasis and mortality [3]. Therefore, significance of the diagnosis rises a lot. With the advances in medical imaging technique, prostate cancer diagnosis methods have also been improved. Despite such technological developments, we are still far from detecting PCa accurately in its early phases, which in turn gives rise to erroneous diagnostic decisions. As a result, there is still ample room for the improvement of imaging techniques and development of novel diagnostic instruments to help mitigate the negative impacts of PCa by providing a more efficient detection method.

Providing an arsenal of contrasts, Magnetic Resonance Imaging (MRI) is one of the most promising imaging tools to build up a powerful PCa detection pipeline. Today, several standards have been set by widely recognized radiology authorities to employ multiparametric MRI for PCa screening (PIRADS) [4]. Moreover, the awareness has been increased about the importance of targeted biopsy techniques despite the presence of a standardized biopsy sampling procedure for prostate [5]. Currently, the most common application of targeted prostate biopsy is carried out by the utilization of ultrasound, a technique that has been referred as Transrectal Ulstrasound (TRUS) [6]. Although this technique is easy to reach, fast and non-expensive, the localization of the target is highly restricted due to low contrast and resolution. This indicates a

need for a more accurate and precise imaging modality to perform targeted prostate biopsy. At this point, MRI is a highly attractive modality given that it provides the highest soft tissue contrast among all imaging techniques without exposing patients to ionizing radiation. Nevertheless, developing biopsy techniques in the presence of a high magnetic field comes with its own set of challenges regarding patient safety and image quality. Recently, researchers has shown an increased interest in the development of targeted prostate biopsy under MRI [5]. However, much of the research up to now has been descriptive in the nature, remaining a need for the design and production of tailored tools to perform targeted prostate biopsy under MRI.

Volume of the biopsy sample is an important factor that determines the diagnostic yield. Therefore, taking more biopsy sample with a single cut is an crucial to increase the efficiency of the procedure. The literature suggests a minimum core length of 11.9 mm for a fairly yielding sampling [7,8]. Hence, not only MRI compatibility and visibility, but also design parameters those determine the efficiency of biopsy procedure should be taken into account.

Based on these, the aim of the present study is developing a novel MRI compatible and visible prostate biopsy needle that provides efficient sampling. Moreover, we also aimed at developing MRI compatible handles to shot these needles efficiently.

MRI compatible prostate biopsy needles that are commercially used in biomedical applications are not MRI visible. Based on the patented needles, materials that are non ferromagnetic like nitinol alloys are used to produce needle but visibility of the needles are inadequate [9]. In line with these reports, noticing the deficiencies of MRI Prostate biopsy procedures during the visit of American Hospital helped us to enhance the properties of the tools that are designed in this project. The prostate needle images and the MRI sequences were taken and evaluated. According to the results, the prostate biopsy needle were not so sufficient to make the process easier and the most important point was the prostate needle was seen as an artifact and hitting the target tumorous location was made by manual adjustments. In this circumstance, it is an important necessity to develop the needle properties and enhance its working

mechanism. The commercial nitinol needle (TSK soft tissue biopsy needle) cannot seen under MRI clearly and location of the nitinol needle can just be estimated because of susceptibility artifact and this situation puts a strain while taking the biopsy. A tunnel that is filled with gadolinium can be seen under MRI that is inserted to the rectum and it helps to determine the location of nitinol biopsy needle. The image that is obtained in the American hospital during the biopsy session is shown in Figure 1.1.
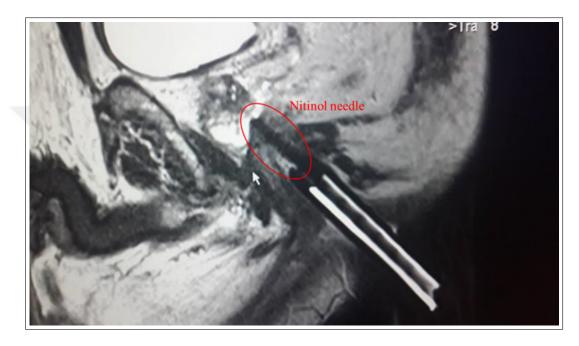
Figure 1.1 Nitinol needle biopsy image under MRI (Courtesy of American Hospital Radiology Department, İstanbul, 2016).

As a conclusion, we aimed to enhance the visibility of the nitinol prostate biopsy needle using iron oxide coating. Different needle tip and biopsy groove configurations are planned to take the target tissue easily with a high yield. Note that commercial prostate biopsy needles are designed using nitinol rod [10]. In this project, we decided to use nitinol wire instead of nitinol rode to increase the efficiency of needle. Moreover, the volume of the biopsy groove is planned to be increased to facilitate sample collection and cutting performance. Finally, we also aimed at producing handle designs with different penetration mechanisms to increase the efficiency of the prostate biopsy needle.

1.1 Anatomy of the Prostate

The prostate, which is approximately 20 g in volume, 3 cm in length, 4 cm in wide and 2 cm in depth [11], is the largest male accessory gland that is located anterior to the rectum and responsible for the secretion of the fluids rich in proteins and minerals that maintain and nourish sperm. It is a pyramidal fibromuscular organ with its shape resembling a chestnut. Regions of the prostate can be classified under five zones as an apex, a base, an anterior, a posterior and two lateral surfaces [12].

Prostate is the origin of two prevalent diseases that are PCa, and benign prostatic hyperplasia (BPH) for elderly men. It is the common cancer type that is commonly diagnosed in aging male population. Today, a considerable part of the health care industry makes remarkable investments in these two prostate diseases and reserve ample funds to research morbidity and mortality in the aging male populations to better understand its mechanisms [13, 14].
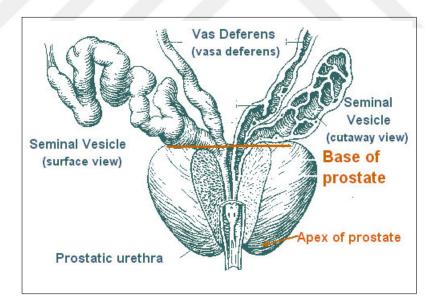
Figure 1.2 Anatomy of prostate [15].

The prostate is divided up into different zones as Central (CZ), Peripheral (PZ) and Transitional (TZ) according to their function. The central zone (CZ) is the part of the prostate that surrounds the ejaculatory ducts and prostatic urethra at the verumontanum. All the prostatic glandular tissue is located in the peripheral zone (PZ).

In accordance with other zones, carcinoma, chronic prostatitis, and post inflammatory atrophy are more common in the peripheral area. The transition zone (TZ) is responsible for development of age-related benign prostatic hyperplasia (BPH) and, less commonly, adenocarcinoma [16].
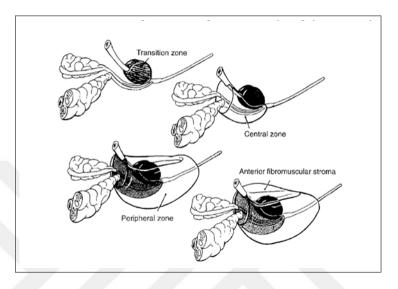
Figure 1.3 Zones of prostate [16].

Transition zone (TZ) contains 5% of the glandular tissue, central zone (CZ) contains about 20%, and the outer peripheral zone (PZ) contains 70%-80% of the glandular tissue. Prostate cancers originate in the peripheral zone (PZ) approximately 70%-75% and in the transitional zone (TZ) around 20%-30%. Central zone is not an origin of cancers; it usually occurs in case of invasion by PZ tumors [17–19].

1.2   Prostate Cancer Screening

Prostate cancer has a high prevalence in aging male population [1] and second cause of death in men [20]. Therefore, an early and accurate detection of the prostate cancer is vital to apply the proper treatment. In many cases, the prostate biopsy is the initial diagnosis technique to detect cancer and evolved over the past 10 years because of the technological advancements and the risks that may occur during the biopsy session has decreased with novel applications. As a result of this, accuracy of prostate cancer diagnosis and successful cancer treatment has improved [21, 22].

Different types of prostate pre-screening methods are explained in the following subsections.

1.2.1 Digital Rectal Examination

In early times of the prostate cancer screening, the examination was made by with finger into a man's rectum to feel for any nodularity, firmness or irregularity in the prostate by a doctor [23].

1.2.2 Transperinal Biopsy (Needle)

It is a technique that takes a sample from the prostate through the perineum via a needle. In 1922, Barringer made the first description of the needle puncturing for acquiring the tissue for histological analysis. The patient was under local anesthesia and sample taken from just lateral to the median raphe 1cm anterior to the anus via 18 gauge needle [23].

The biopsy technique gives us an opportunity to take the tumorous tissues that are at the apex and anterior zones. These zones are common sites for prostate cancer detection [24].

1.2.3 Transurethral Biopsy

Transurethral biopsy of the prostate is a method that requires general anesthetic, and the needle reaches to the prostate gland from the way of the urethra.

According to pathological examination results cancer is detected in 53 men which is 12.5%. For detection, the transurethral biopsies are used and they achieved to detect 32 of 53 (60.4%) which means transurethral biopsies missed the 21 cancer case. We

can conclude that transurethral biopsy sampling is not efficient and reliable to detect prostate cancer in men with clinically significant BPH [25]. Additionally, in another research it is demonstrated that transurethral biopsies are not useful in patients with frequently elevated or increasing serum PSA [26].

1.2.4   Transrectal Approaches

Transrectal approach uses different types of needles to reach the prostate gland via rectum and collect the tumorous tissue.

- **Needle:** Below figure shows an early design of a fine needle and a guide [27].
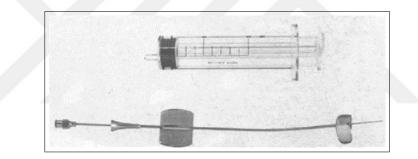
Figure 1.4 The needle and guide with disposable syringe [23].

- **Digitally guided transrectal biopsy:** Finger guided biopsy techniques was very common up to 1950s although Astraldi made the first transrectal Digital-guidance biopsy in 1937. In 1959, Barnes and Emery used the sound of urethra to diagnose the prostate cancer via placement of the Silverman needle [23].

1.2.5   Prostate Specific Antigen (PSA)

Prostate-specific antigen (PSA) is a protein produced only by prostate cells and valuable cancer indicator. PSA test used to determine the volume of PSA within the blood. If the volume of PSA is higher than normal values (<4 ng/mL), it means prostate cancer may be present. Number of systematic biopsies shows that cancer
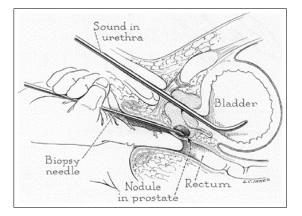
Figure 1.5 Digitally-guided transrectal biopsy of the prostate with the sound of urethra [23].

detection level of PSA is 10 ng/mL or in patients with prostate sizes 50 cc [21, 28, 29]. However, PSA is insufficient to warrant to diagnose the prostate cancer based on current evidence [1].

1.2.6 The Sextant Method

In 1989, two papers published in the Journal of Urology by Hodge et al. has started the modern era of the prostate biopsy needle [30]. First article described the transrectal prostate biopsies of palpable abnormalities and the second paper, which started the new era of the prostate needle biopsy, described the schematic biopsy that divides prostate into six sites the apex, middle, and base of each prostate lobe. According to the information gathered by accumulation of the literature, this method is considered as successful to detect the prostate cancer [23]
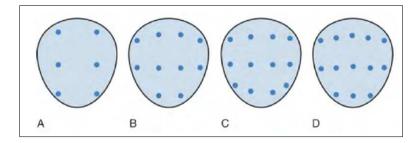
Figure 1.6 Different systematic biopsy schemes. A) Sextant biopsy, B) The 10-core biopsy, C) The 12-core, or double sextant biopsy, D) The 13-core, 5-region biopsy [23].

1.3 Imaging Modalities for Prostate Biopsy Procedure

1.3.1 Transrectal Ultrasound (TRUS) Guided Biopsy

It is a technique to create an image of the prostate on a video screen by a small probe that produces sound waves. The information of echo is translated by a computer into a picture to determine the normal and abnormal areas of the prostate. The men with an abnormal DRE, a high level of PSA (>4.0 ng/ml) or PSA velocity (rate of PSA change) >0.4 to 0.75ng/ml/yr is highly at risk of prostate cancer, and TRUS-guided prostate needle biopsy should be performed [31].

Transrectal biopsy usually need to 8-12 samples from various locations to diagnose the prostate cancer due to an acceptable protocol based on published data [23,32,33]. However, the accuracy of the detection is controversial due to the prostate gland size variations. According to Karakiewicz et al., the bigger the size of the prostate gland, the lower the yield of sextant of biopsy [34].
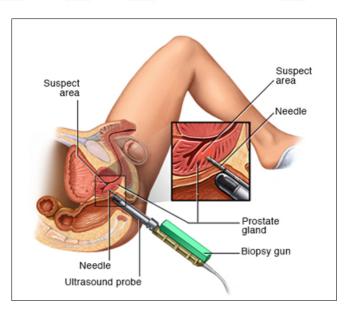
Figure 1.7 Illustration of transrectal biopsy procedure [35].

In addition, TRUS technique also has some disadvantages that cause false positive results. Low resolution and low contrast of images decrease the success of the diagnosis. Images helps the physician while taking the biopsy from the suspicious area

with a thin needle, so visibility of the cancerous tissue and determining of the suspicious area is a key to increasing the success of the diagnose.

After the development of ultrasound imaging, the first trans-rectal ultrasound guided prostate biopsy described by Takahashi and Ouchi in 1963 although the quality of the image was too poor. Association with technological progression towards the 1980s, high-quality apparatus like 7 MHz probe has been produced and enabled to obtain better diagnosis [23, 36].

The disadvantages of sonography is detecting the tumors that are tend to be larger, therefore a monitor and extra features is required for sonography to detect the prostate cancer in an early stage. Based on the technological developments ultrasound technique also has developed and yield of prostate biopsy increased [37]. Enhanced ultrasound modalities (EUM) such as color, power Doppler, contrast-enhancement, harmonic and flash replenishment imaging, and elastography play essential role in detection of prostate cancer [38].

1.3.2   Computed Tomography (CT) Scan

CT is a transmission based imaging technique that reconstructs multiple X-ray projections to provide high-resolution anatomical images. Although it provides rapid image acquisition for low costs per scan, target is exposed to ionizing radiation, which has been a matter of debate for a long time regarding public health [39]. Moreover, X-ray attenuation does not yield a satisfactory soft tissue contrast. Therefore, utilized alone CT is not an efficient modality for the detection and the grading of the PCa. Sole application of CT in PCa detection is confined to the identification of enlarged lymph nodes [40]. In clinical practice, CT is commonly combined with Positron Emission Tomography (PET/CT), which is a nuclear emission based imaging technique that localizes the source of excessive metabolic material uptake upon the administration of radiopharmaceuticals. Depending on the selected radiopharmaceutical, PET/CT is shown to be either discouraging [41] or not suggested as a first-step screening method

especially for high-risk groups in PCa [42]. Overall, CT cannot be regarded as a promising imaging modality for the detection and the classification of PCa.

1.3.3   Magnetic Resonance Imaging (MRI)

MRI is a non-invasive imaging technique consist of a magnet, magnetic gradient coils, an radio frequency transmitter and receiver and a computer. It uses absorption and emission of radiofrequency energy and manipulates magnetic fields systematically along three axes. Therefore, it does not need to reposition the target anatomy and provides images in different planes. Although MRI has many advantages including superior soft tissue contrast, prostate imaging comes with its set of challenges.

The prostate has a small anatomy and located in the central region of the body, which lowers SNR. Moreover, it is ensheathed by a lipid pool. Given that PCa is commonly observed in the peripheral zone [43] special measures must be taken to avoid detrimental effects of the chemical shift interference especially for susceptible modalities such as MRS. To overcome these problems, different techniques have been developed for decades. A common solution to elevate SNR level to acceptable levels is combining phased array coils with endorectal coils. This combination has been shown to detect more cancer foci in diffusion weighted prostate images [44]. Moreover, sophisticated imaging sequences have been designed to provide a more accurate prostate localization for MRS [45]. Despite its promising potential for use, MRS has not taken its place in clinical practice yet in multimodal prostate MRI [46]. A commonly referenced guideline by American College of Radiology, Prostate Imaging Reporting and Data System (PI-RADS), suggests a multiparametric approach for the detection and characterization of PC [4]. These MR modalities are T2 weighted, diffusion-weighted and dynamic contrast-enhanced imaging (DCE).

T2w imaging is one of the most basic imaging sequences in MRI that displays anatomy regarding the differences in the T2 relaxation times of tissues. In this regard, the detection of the tumorous tissue in the prostate is bounded by the degree of dif-

ference between healthy and pathological tissue. It has been shown that T2w images have a low accuracy for this purpose since malign prostate tissue characteristics can be resembled by other diseases [47]. Have demonstrated that performance of diffusion imaging in detection is more reliable than that of T2w images. Nevertheless, T2w contrast is still contained in the prostate imaging procedures since it has the ability to provide morphological anatomy with high resolution.

As it has provided a new dimension to the detection of brain tumors and led to the emergence of human connectome studies [48], diffusion imaging has acquired an important role also in the prostate imaging [49]. Unlike the T1 and T2 weighted images, contrast in diffusion imaging is determined according to the restriction of the microscopic motion of the water molecules in certain directions. This is achieved by applying diffusion sensitizing gradients in multiple directions (at least six), and modeling the diffusion characteristics for each voxel as a tensor [50]. From these tensors, several diffusion anisotropy indices are calculated including fractional anisotropy (FA), mean diffusion (MD) and apparent diffusion coefficient (ADC) maps, etc. [51]. This metric has been shown to be effective in differentiating benign tissue from malignant tissue in peripheral PC [44, 52] and highly recommended by PIRADS guideline for the imaging of PC in the peripheral zone.

Lastly, DCE imaging is a special MRI technique which is based on the administration of contrast agents to delineate tumors and vascular networks better [53]. Image reconstruction is designed to exploit the fact that contrast agent-based dynamic changes will appear only in a certain region of the raw data, so that fast and effective acquisitions are possible. Being one of the three imaging modalities for multiparametric imaging of prostate in PI-RADS guideline [35], DCE has been shown to be a suitable approach for the detection and grading of early PC [54].

As a conclusion, MRI is a powerful imaging technique for an accurate detection and grading of the PCa thanks to its wide spectrum of contrasts, being non-invasive without exposing ionizing radiation and ceasing the need for target repositioning to acquire images in different planes.

1.4   Grading of the Prostate Cancer

After the prostate biopsy sample, if it is diagnosed as cancer, it is classified according to its aggressiveness. The most common grading system is Gleason system. It is based on a comparison of cancer cells with normal prostate cells. Gleason score (range of 2 to 10) can be obtained by adding two grades to each other; first grade represents 'most like normal cells' (through 5) and the second grade represents 'least like normal cells' (through 5). The Gleason score is essential to determine the treatment because tumor grade is an important factor to detect the aggressiveness of prostate cancer [16].
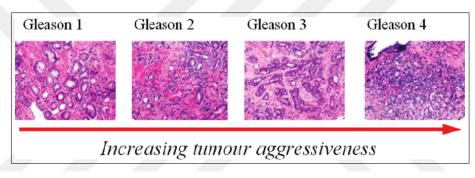
Figure 1.8 Examples of the prostate tissue sections with different Gleason scores (size about 700 by 900 μm^2) [55].

1.5   Prostate Biopsy Under MRI

Although most of the prostate cancer screening comprises several challenges, MRI guided biopsy provides more reliable solutions with localizing significant tumors [56].

Some of the advantages of MRI in PCa screening can be listed as follows:

- Reduced number of biopsies (less bleeding, pain, infection risk)

- Detailed anatomical images (less false positive results)

- More precise tumor targeting, rapid and accurate diagnosis [56]

MRI can be used to improve treatment planning for prostate carcinoma by providing information that not only helps to more accurately delineate the prostate and seminal vesicles, but also to define a subtarget within the prostate that can be treated to a higher dose [57].

We attended prostate biopsy sessions that was committed under MRI at American hospital. According to our observations, first thing was preparing and positioning the patient and after that immobilizing the base plate (DynaTrim). Second thing was obtaining the image of prostate gland and detecting the tumorous tissue. Rotation, angulation and movement was measured with a program that is called DynaCAD after obtaining the image of prostate. This program helps the physician to determine the angle of needle and distance of needle from the tumorous tissue for shooting. After detection of the required parameters, needle inserted to the patient's prostate gland with specified angled via the tunnel that is inserted to the patient's rectum. After positioning the needle, the physician shot the needle to take the tumorous tissue and after that withdrew the needle. All these adjustments performed manually by technicians and physicians.
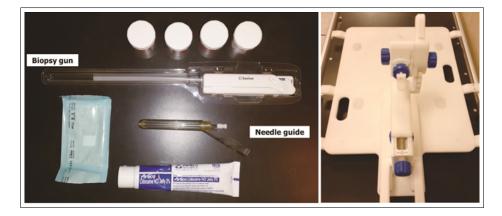
Figure 1.9 Equipment that are used under MRI prostate biopsy a) biopsy gun, prostate needle guide, bottles and lidocaine jelly, b) base plate (Invivo, Schwerin, Germany) [58].

1.6   Visibility of the Devices Under MRI

Visualization of the devices that are used under MRI is still the topic of active research for interventional applications. There are two different approaches to deal with this problem, active tracking and passive tracking. Active tracking devices are the ones that are equipped with an electrical hardware. These methods use RF coils that are attached to the device or alters magnetic susceptibility via induction. Unlike active tracking instrumentation, passive tracking does not include any kind of active hardware. This means that the whole body of the device can be seen under MRI without the need of any electromagnetic manipulations. As a result, passive markers cause less heating of tissue caused by RF.

One of the passive tracking methods is positive image contrast. This technique uses a dilute solution of MR contrast agent, filling the catheter lumen to increase the visibility of the device. Herewith, the device emits the signal and brightens under MRI. Using a similar approach, an alternative solution is to minimize the background tissue signals to enhance the visibility of the device. There are several methods to suppress this signals such as Hadamard excitation pulses [59], the projection dephaser (PD) [60], magnetization preparation [61].

The advantage of employing the PD method stems from the fact that tissue signal can be efficiently suppressed using magnetic field gradients with small amplitudes [62]. The extent of the application of the projection cycle determines the degree of suppression. For example, to reach a uniform background, a full cycle projection must be applied. Regarding the fact that devices occupy more less volume in the excitation area, the effect of dephasing will be insignificant on the device, which eventually increases the relative signal acquired from it. To extend this conventional way of conspicuity enhancement of the device, Draper et al. has suggested a multi-cycle approach rather than single cycles [63]. This method has increased contrast by a factor of ten, where measurements are performed using the following device-to-background contrast (C) equation:

$$C = \frac{S_c - S_b}{S_c + S_b} X 100\% \tag{1.1}$$

where S_c is the signal from device and S_b is the signal from the background tissue.

1.7 Existing Needle Designs

Current biopsy needles that are used in biomedical applications have different tip configurations with several cutting mechanisms and variable handle designs. There are more than one possible categorization of the needles regarding their cutting mechanisms. Nevertheless, it is possible to consider two main categories based on cutting mechanisms, which are the end cutting and the side cutting. Although end cutting needles just have a sharpened hollow tube to cut and take the tissue, side cutting needles uses a sliding sheath for cutting mechanism. The literature indicates that side cutting needles can push the tissue rather than taking. End cutting needle, on the other hand, can core out the tissue around the target area. This highlights the importance of decision making about the cutting mechanism in the efficiency of the biopsy procedure.

Two other important design parameters are needle diameter and tip type. Needle tips include conic, bevel and blunt tips [64]. Comprehensive testing on the effect of needle diameter and tip type on the mechanics of the insertion has shown that needles with bevel tips are more likely to experience bending and larger diameters increase friction [65]. This in turn results in more forces to act on the needle. Moreover, analytical modeling of the needle tip and cutting angles has identified these parameters as a prerequisite knowledge for making a needle design [66]. Highly relevantly to the present study, studies reviewed here suggest testing different tip and cutting designs in the development process of a biopsy needle.

2.   METHODS

2.1   MRI Compatible Prostate Biopsy Needle

2.1.1   Selection of the MRI Compatible Material

Nitinol is commonly used in biomedical applications because of its material properties especially being MR compatible. In addition, nitinol has shape memory effect that describes restoring the original shape by heating and pseudoplasticity that means recovering the original shape after large deformations [67].

Moreover, the properties of nitinol like elastic deployment, kink resistance, thermal deployment, bio-compatibility, superelasticity, constant unloading stresses, fatigue resistance, uniform plastic deformation are also remarkable for selection of needle material [10]. Nitinol also has a lower magnetic susceptibility compare to stainless steel, therefore it is safe to, and it provides more clear images with fewer artifacts [67].

Nitinol is commonly used as stent, retrieval baskets, intra-aortic balloon pump, endoscopic instruments use nitinol rods to actuate scissors and graspers, the atrial septal occlusion device, the arrow inter-aortic balloon pump, etc. after commercialized in the biomedical industry [10].

2.1.2   MRI Compatible Prostate Biopsy Needle Design

The distal tip and biopsy reservoir geometry of the nitinol biopsy needle set (outer and inner needles) were designed by using Solid Works 2015 CAD software as shown in the figure 10.
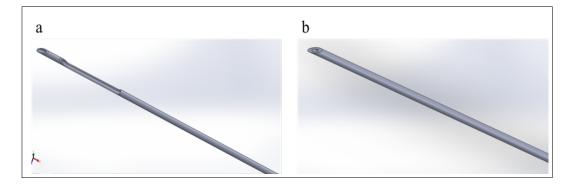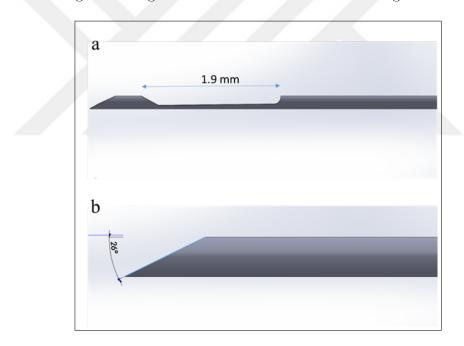
Figure 2.1 Prostate biopsy needle design on SolidWorks 2015 a) Inner needle (1.38 mm OD / 0.93 mm ID) b) Outer needle (2.05 mm OD / 1.47 mm ID).

The design and lengths of inner needle are shown in Figure 2.2.

Figure 2.2 a) Inner needle lengths (27 cm length and 1.9 mm length biopsy groove) b) outer needle (22 cm length and 26° tip angle).

Both inner and outer needle drawings converted to flat geometry from tubular geometry on Solidworks 2015 and converted to DWG format to transfer the laser cutting device. The flat images of the needles are shown in Figure 2.3.
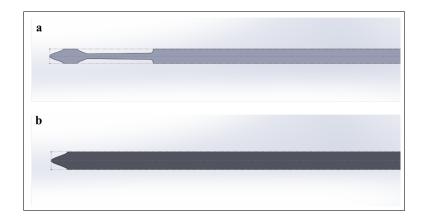
Figure 2.3 Tubular to flat geometry conversion of needles a) Inner needle b) Outer needle

2.1.3 The Biopsy Mechanism Design of the Needle

The prostate needle has been designed by using MRI-compatible material such as nitinol. It consists of two needles (inner needle and outer needle) which have completely different shapes and working mechanisms. There are two interwoven needles in our design. The outer needle is used as a guide while inserting and pushing forward in the prostate gland via rectum. Inner needle is used as carrierg via taking the tumorous tissue into its biopsy groove. When both needles are inside the prostate gland, inner needle is advanced to the exact tumor location, the outer needle is shoot to cut the tissue and the biopsy sample is locked in biopsy groove of inner needle. Finally both needles are withdrawn from the body.
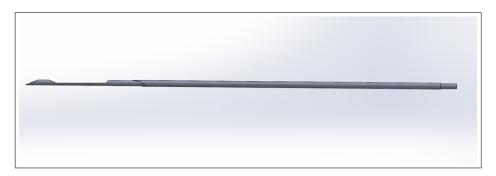
Figure 2.4 Prostate biopsy needle solidworks design (inner and outer needle).

2.1.4 Fabrication of the Biopsy Needle Prototypes

Biopsy needle was designed in SolidWorks 2015 (Dassault Systemes SOLID-WORKS Corp, ABD) and converted to the format required by laser cutting system using Alphacam (Vero Software, UK). Laser cutting of the biopsy needle was carried out using Nd:YAG (neodymium-doped yttrium aluminum garnet; Nd:Y3Al5O12) laser cutting device, which is located at the Life Sciences and Technologies Research Center, Boğaziçi University. This device has a maximum power of 400 W and 18-20 micron beam diameter. To prevent oxidation and overheating during laser cutting process, argon gas and water-cooling system were utilized, respectively.

Firstly, required modifications and transformations were on the laser cutting device to change its utilization settings from plate cutting to tube cutting. To enable this, all required additional parts were 3D printed in Life Sciences and Technologies Research Center, Boğaziçi University. After bringing laser cutting device compatible with nitinol tube dimensions, biopsy needle cutting was performed. Following this, to enable sufficient mechanical strength and easy tissue penetration characteristics of biopsy needles, different inner needle geometries were designed and produced using this modified setup. The laser cutting device is shown in the Figure 2.5.
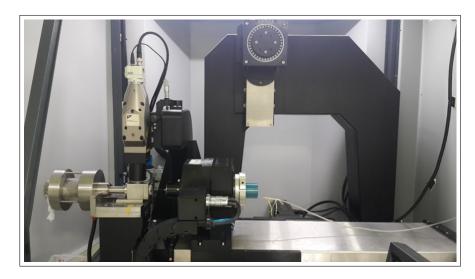
Figure 2.5 Laser cutting device.

2.1.5 Surface Treatment

The oxide and notch layer that consist of laser cutting has been removed via micro-blasting. Micro-abrasive blaster (COMCO INC. AccuFlo) and 50 micron aluminum oxide precision micro abrasive powder has been used to remove the notches.
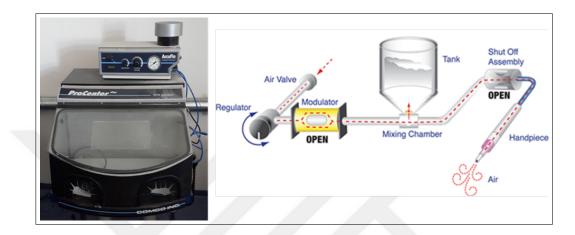
Figure 2.6 Microblasting device and working mechanism [68].

Microblasting device has air valve regulator modulator, mixing chamber, tank and handpiece with different size nozzles when other modulator is opened, the tank fulfills with air pressure (70-90 psi) that passes through mixing chamber. This high pressure air fluidizes the small amount of abrasive. After closing the modulator the high air pressure that is entrapped into the tank is released due to the decreased pressure in the mixing chamber and the fluidized abrasive is released from tank and erupts from the handpiece and removes the notches. Modulator opens and closes 60 times per second. The images after and before microblasting are shown in the Figure 2.7.
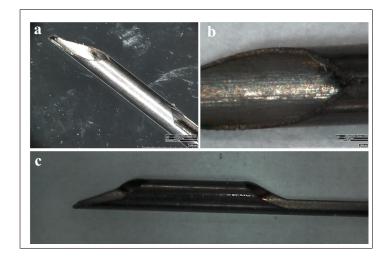
Figure 2.7 Nitinol biopsy needle a-b) before microblasting and c) after microblasting.

2.2 Forming Passive Visualization Markers on Biopsy Needles

2.2.1 Iron Oxide (Fe$_2$O$_3$) Markers

Iron oxide (Fe$_2$O$_3$) is a compound that is found in nature as a natural mineral magnetite. It contains iron ions and shows permanent magnetic feature and also it is ferromagnetic. Recently, mangnetic nanoparticles synthesis are extensively studied and superparamagnetic iron oxide nanoparticles grab researched attention because of its easily penetration and contrast enhancement properties. Iron oxide magnetic nanoparticles (IOMPs) are getting popular and also some medical products which are based on this material received their approval from US FDA such as Sinerem (Guerbert), Clariscan (GE Healthcare), Endorem (Guebert), Resovist, Abdoscan (GE Healthcare), and Lumirem (Guebert) since they are suitable for imaging different locations such as liver, spleen, bone marrow and lymph nodes [16, 69].

In order to achieve imaging, IOPMs' contrast enhancement in magnetic resonance imaging property is utilized. However, in this project we used iron oxide nanoparticles as coating to enhance our visibility of the prostate biopsy needle.

As a solution of prostate needle biopsy visibility enhancement, iron oxide nanoparticle coating was considered over the outer needle surface. MRI visible distance markings were placed on the nitinol needle at certain intervals by circumventing them using Iron (II-III) oxide (Fe_2O_3) coatings. In this way, a real-time passive localization of the biopsy needle with respect to the tumor location was intended to provide an easier biopsy procedure. Thickness of each coating and coating intervals were determined to equal 1 mm and 5 mm, respectively. Iron (II, III) oxide nano-powder (Aldrich Chemistry, 5 nm diameter) was mixed with ultraviolet (UV) cure solution (Dymax medical device adhesives and coatings, 204-CTH-F) 3 ML and applied on nitinol needles with the help of the polyamide masking bands that are placed at regular intervals of 5 mm, using a fine brush. Next, needles were exposed to UV light for 200 seconds to fasten coatings onto needles. The results are shown in Figure 2.8.
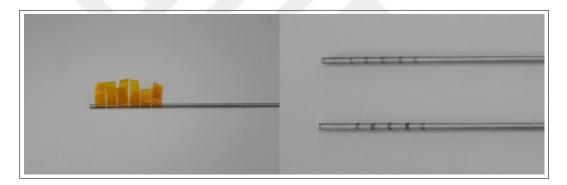
Figure 2.8 Iron oxide nanoparticle coating (135 ± 5 μm thick) with polyamide tape masks.

Different concentration values were prepared to determine the most appropriate concentration value, and the images which are obtained and tested under MRI were compared. The concentration values of the prepared solutions are as shown in Table 2.1.

Table 2.1
Concentration of the prepared solution.

Sample	Iron Oxide (gr)	UV Solution 3ml (Drop)
1	0.04	4
2	0.02	4
3	0.01	4
4	0.005	4
5	0.0025	4

Figure 2.9 Images of iron oxide coated outer needles coated different concentration.

2.3 Mechanical Tests

2.3.1 Stiffness Tests

Produced biopsy needles were mechanically tested to determine an appropriate design for biopsy procedure using digital force meter. Each needle was fixed from its proximal end (blunt end) and gradually pushed towards a silicon material until the needle was penetrated in and proceeded a certain distance (1 cm). During this process, axial force acting on the needle was recorded and deformation was observed.

Figure 2.10 Stiffness testing mechanism (LLOYD instruments, LF Plus digital testing machine).

2.3.2 Peeling Tests

An adhesive tape was used to prove the adhesive power of iron oxide coatings. The tape was pasted to the surface of coatings and withdrew. According to results, iron oxide nano-coating was durable enough for the first trials.

2.4 Prostate Biopsy Gun Design of the Biopsy Needle

Two different prostate biopsy needle guns have been designed in Solidworks 2015 to take the target tissue easily and successfully each time. Produced biopsy needles (inner and outer needles) were nestled and placed within two different handle designs fabricated through 3D printer (Zortrax M200). First handle design is a conventional gun that has straight pin channel. The second handle design is a spiral gun that has a spiral pin channel (two ends of the groove are 180° apart). Both designs include a stainless steel compression spring to fire the outer needle to perform the biopsy procedure. As a working mechanism of the gun, the inner needle is attached to the back of biopsy handle. The outer needle is attached to the piston that can move back and forth throughout the handle. The pin is attached to the piston to manipulate it. When the pin moves back and forth during the pin channel, piston and outer needle

also moves and piston compress the spring. According to action mechanism, when the pin is not locked the spring is released, when the pin is locked, the spring is squeezed. The spring is produced using 7 mm stainless steel compression coil (7 cm length and 1 mm diameter) and becomes 3 mm length after squeezing 4 mm. After that, to prevent the undesired releasing, lock the pin to immobilize the spring. When the inner needle groove is on exact location based on MRI images, unlock the pin, release the spring that fires the outer needle. Therefore, the outer needle slides on the inner needle and takes the expected tumorous tissue sample into the biopsy groove. The difference between the first and the second design is the spiral movement of the outer needle. Spiral biopsy gun gives an angle to the outer needle while sliding on the inner needle. It is expected to cut the tissue easily while sliding rotationally on the inner needle. Both handle designs are shown in Figures 2.11 and 2.12.
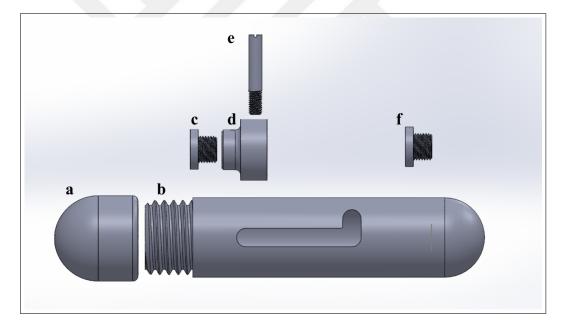
Figure 2.11 Conventional prostate biopsy needle gun a) handle cap b) needle handle c) bushing of outer needle d) piston for spring e) pin f) bushing for inner needle.
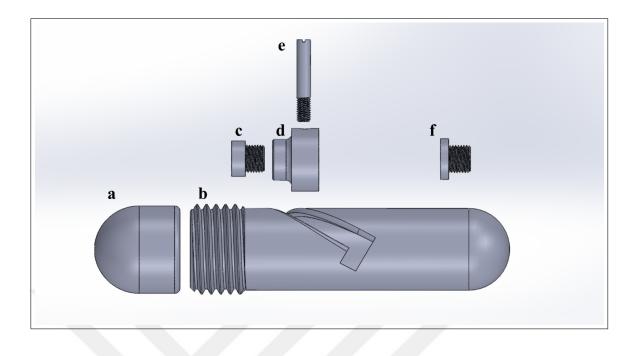
Figure 2.12 Torqued prostate biopsy needle gun a) handle cap b) needle handle c) bushing of outer needle d) piston for spring e) pin f) bushing for inner needle.

The handle designs were fabricated by using a three dimensional printer (Zortrax M200 3D printer) Z-ultrat thermoplastic filament was used as a printer material. The printed and unified model of the guns are shown in the Figures 2.13 and 2.14.
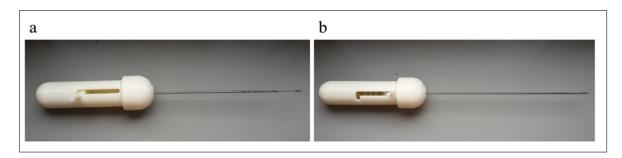
Figure 2.13 Conventional prostate biopsy needle gun a) before shooting b) after shooting.
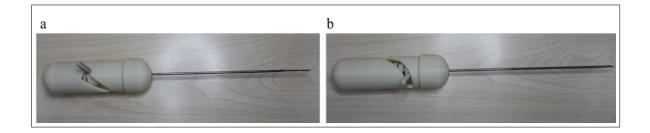
Figure 2.14 Torqued prostate biopsy needle gun (180° angle) a) before shooting b) after shooting.

3. RESULTS

3.1 Biopsy Needle Production Using Laser Cutting

The biopsy needle design has two coaxial needles to increase the biopsy efficiency of the needle. The aim of this design is: have sharp outer needle tip to reach the tumorous area easily, take the target value of cancerous tissue, cause less bleeding, less traumatic cutting, prevent the fracture of the needle during the procedure especially when it is inside the body and prevent the damage of the tissue.

Using laser cutting technique, multiple needles have been produced from different designs and their conveniences have been evaluated. Given that the inner needle is relatively more functional and attaining less mechanical strength in comparison to outer needle, more tests and designs have been carried out for it. Part of these designs is shown in Figure 3.1.
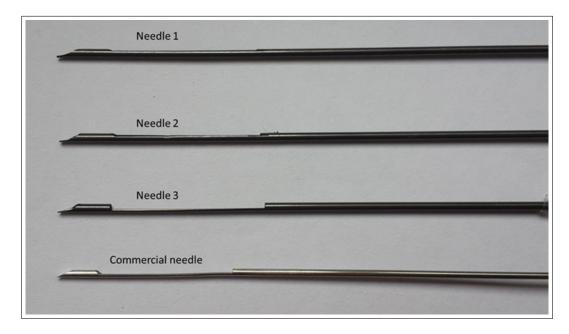
Figure 3.1 Biopsy needles with 1) high walled biopsy groove with less pointed tip, 2) high walled biopsy groove with a pointed tip, 3) pointed tip and low walled biopsy groove with a pointed tip. A commercial needle used as a reference (TSK soft tissue biopsy needle).

The nitinol needles with high-walled biopsy grooves (design 1 and 2) attain higher forces at the moment of puncture and deflect less than the needle with low-walled biopsy groove (design 3) does. Figure 3.2 shows that the insertion forces for nitinol biopsy needles with high-walled grooves are comparable to conventional biopsy needles.
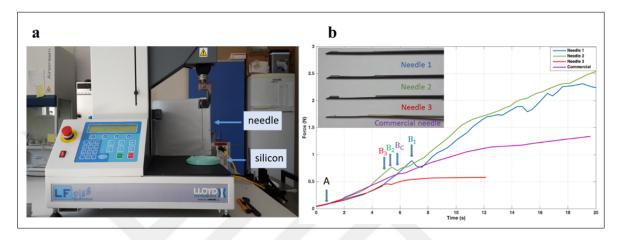
Figure 3.2 a) Mechanical testing apparatus for biopsy needle penetration test. The samples inserted into a silicon mold at a constant speed of 5 mm/sec. b) Needle insertion forces measured by load cell with high-walled biopsy groove and less pointed tip (Needle-1, blue), high-walled biopsy groove and pointed tip (Needle-2, green) and low-walled biopsy groove with pointed tip (Needle-3, red). A commercial needle used as a reference (TSK soft tissue biopsy needle, purple). Initial needle peak insertion forces (N): 0.89, 0.77, 0.46, 0.64 and peak time points (s): 6.83, 5.40, 5.01, and 5.92 for needle 1, 2 and 3 and commercial needle, respectively. A indicates the time point when the needle contacts the mold surface B indicates the time of puncturing for each needle.

3.2 Prostate Biopsy Handle Gun In Vitro Trials

The performance of the unified biopsy mechanisms were tested in vitro using fresh veal meat as shown in Figure 3.3. The obtained results are shown in Figure 3.4.

Figure 3.3 Demonstration of in vitro biopsy trials with fresh veal meat.
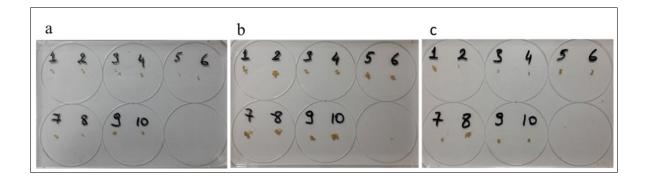
Figure 3.4 Biopsy samples that are taken with a) the commercial needle (TSK, soft tissue biopsy needle) b) the conventional prostate biopsy needle gun c) Spiral prostate biopsy needle gun.

Table 3.1
Biopsy sample weights measured with microscale (Mettler Toledo, MS TS balances).

Sample Number	Commercial Needle (gr)	Conventional Needle (gr)	Spiral Biopsy Needle (gr)
1	0.0008	0.0039	0.0034
2	0.0008	0.0062	0.0008
3	0.0002	0.0032	0.0009
4	0.0002	0.0016	0.0020
5	0.0001	0.0039	0.0018
6	0.0003	0.0022	0.0015
7	0.0006	0.0045	0.0036
8	0.0004	0.0038	0.0014
9	0.0004	0.0032	0.0009
10	0.0004	0.0061	0.0017
Average	0.00042	0.00386	0.0018

The weight of tissue biopsies was measured with microbalances, and the average weights were calculated as 0.00042 gr, 0.00386 gr and 0.0018 gr for a commercial needle, the conventional prostate biopsy needle gun and the Spiral prostate biopsy needle gun, respectively. The standard deviations for commercial biopsy needle gun, conventional biopsy needle gun and for spiral prostate biopsy needle gun are 0.000244, 0.0015 and 0.000984, respectively.

Designed prostate biopsy needle diameter is thicker than commercial prostate biopsy needle diameter. Designed prostate biopsy needle groove volume (9.05 mm^3) is almost two times bigger than commercial needles groove volume (4.72 mm^3), however when examined the average weights of the biopsy samples for inner needles, the difference between weights of biopsy samples that are taken during in vitro trials is bigger than two times. The different design characteristics of produced needles may lead to this distinctness. Designed inner needle has high walled biopsy groove and also needle wire is used instead of nitinol rod with difference of the commercial needle. That might

have formed basis for obtaining more tissue with minimum loss. High walled nitinol wire needle may enable obtainment of relatively larger biopsy samples with less slot volume.

3.3   Iron Oxide (II-III) Coated Nitinol Needle under MRI

Effect of Fe_2O_2 concentration on T2 weighted MR images acquired by TSE sequence at 1.5T is shown in Figure 3.5. In the regions where coatings are present, expansion of the hyperintense regions is observed to be higher for coatings with high concentration, compared to those with low concentration. A plausible expectation for the measurement of the thickness of each coating and the distance between two coatings are expected to fall within 1-2 mm and 3-5 mm, respectively. Distance measurements performed on MR images of nitinol needles with high concentration coatings indicates 1.67 ± 0.36 mm (mean $\pm$ SD) of coating thickness and 4.53 ± 0.12 mm of coating intervals. Minimum coating thickness equals 1.67 ± 0.36 mm for the coating with the lowest concentration. Note that this value converges to expected values better than the remaining. However, boundaries of hyperintense regions in coatings with low concentrations are not possible to be distinguished as clearly as in the coatings with higher concentrations. Since this challenges a consistent determination of the coating intervals (5.42 ± 0.12 mm), accuracy of the measurement seems to decrease. On the other hand, measurements performed on the coating number 3 that attains a moderate concentration result in values (4.82 ± 0.3 mm) converging to the actual dimensions better than the remaining does (Figure 3.6). Moreover, moderate concentration allows the expansions of the hyperintense regions remarkably, which increases the accuracy and the repeatability of the measurement.
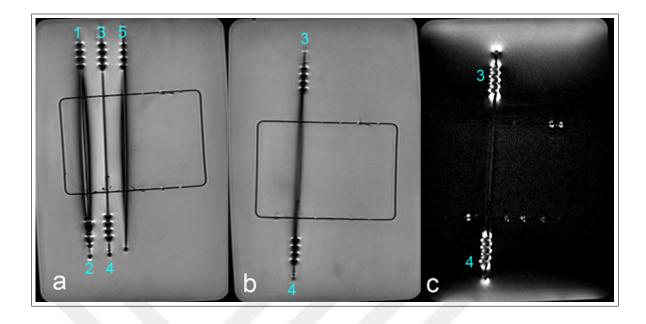
Figure 3.5 T2 weighted MR images acquired using Turbo Spin Echo (TSE) imaging sequence: a) All nitinol needles that are coated by Fe_2O_3 compound with different concentrations (1: maximum concentration 5: minimum concentration) at identical intervals of 5mm, b) image of the nitinol needle with coatings number 3 and 4, c) image (of the nitinol needle with coatings number 3 and 4 for) acquired by changing phase encoding direction and applying water suppression.

Distortions caused by the selection of the phase encoding direction along the long axis of the needle preclude the feasibility of distance measurements. (Figure 3.5-c). The needle having the coatings number 3 and 4 shows fewer distortions when compared to the remaining needles (Figure 3.5-a). To eliminate the effects caused by possible magnetic susceptibility interactions due to the presence of other needles on the appearance of the image, this needle was imaged for the second time using same acquisition parameters (Figure 3.5-b). When imaged alone, distortions on the needle shaft has been shown to increase drastically.
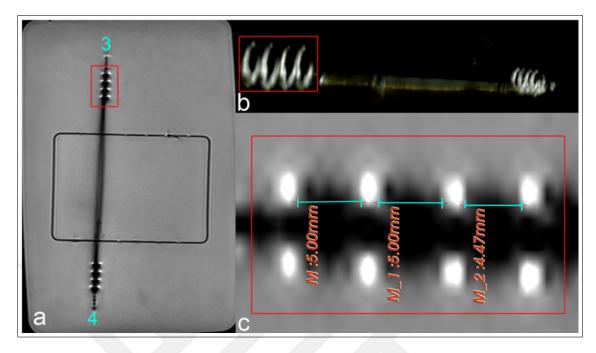
Figure 3.6 MR images acquired using TSE sequence belonging to the nitinol needle which has coatings number 3 and 4 on it. Red frames indicate the area corresponding to the same region in all panels. a) T2 weighted MR image, b) 3D image reconstruction of biopsy needle (ring-shaped structures represent Fe_2O_3 coatings), c) measurement of the coating intervals.
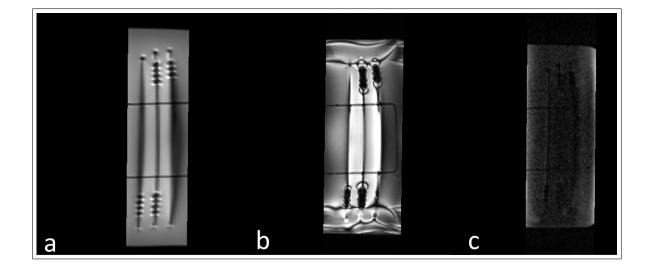
Figure 3.7 MR images in each panel are acquired with different imaging sequences, showing three biopsy needles having coatings with different Fe_2O_3 concentrations. a) Image acquired by (spin-echo based) Half-Fourier Acquisition Single-Shot Turbo Spin-Echo (HASTE) sequence, b) image acquired by (gradient-echo based) Fast Imaging with Steady State Precession (FISP) sequence, c) image acquired by (gradient-echo based) Volumetric Interpolated Brain Examination (VIBE) sequence.

4. DISCUSSION

Different prostate biopsy needle designs with needle tip and biopsy groove configurations were fabricated and their performance was compared through in vitro tests. Obtained samples indicate that Nd:YAG laser cutting can be successfully utilized in nitinol needle production. Outer needle tip angle was sharp enough to cut the tissue, but the most challenging part of the design was determining the inner needle biopsy groove design that is both durable and efficient. Due to the property of superelasticity of nitinol, designing inner needle biopsy groove with different wall thicknesses was expected to give us ideas about nitinol durableness for use of the project. Stiffness of nitinol is less than stainless steel and the elastic range is almost double compared to stainless steel, therefore the inner needle can bend during insertion of the tissue and the angle of needle tip can change [70]. This causes the misplacement of needle and makes difficult to take the target tissue, false results increases and yield of biopsy decreases. Two different biopsy groove with high walled and low walled were decided to produce for the inner needle. According to bending test results, inner needle with high walled biopsy groove shows more durable characteristic than the inner needle with low walled biopsy groove. Based on the results, we decided to generate the needle with high wall.

Distance measurements performed in the acquired MR images reveal a proportional relation between the coating concentrations and the precision of the measurements. On the one hand, high Fe_2O_3 concentration cause coating intervals to be underestimated, on the other hand, it increases the noticeability of the hyperintense regions, facilitating the real-time passive tracking. However, it is worth bearing in mind that the more the ferromagnetism is pronounced, the more prominent artifacts will occur. Therefore, Fe_2O_3 coatings with moderate concentrations appear to be an optimum preference for the passive tracking of penetration depth.

Figure 3.5 shows that distortions are occurring in the biopsy needle MR images depend not only on the concentration of ferromagnetic coatings, but also on the se-

lected phase-encoding direction of the acquisition sequence. It has been reported that aligning frequency-encoding direction with the long axis of the needles reduces metal susceptibility artifacts [71]. This is in good agreement with the present findings, highlighting the importance of reserving the appropriate direction for frequency encoding before acquiring images. In addition, distortions observed on the shaft of the biopsy needle having the coatings number 3 and 4 show an increase when the needle is imaged alone (Figure 3.5-b). Improvement in the image quality (Figure 3.5-a), occurring when the needle is placed between of the remaining needles can be therefore ascribed to a possible neutralization of the susceptibility effects, which is most likely to be caused by concomitant electromagnetic interactions.

Although utmost care was taken to adjust gradient-echo based sequence parameters in this manner, images acquired by spin-echo based sequences are superior to those acquired by gradient-echo based sequences in the distinguishability of coatings, in all cases (Figure 3.7). This is because spin-echo based sequences utilize refocusing pulses that have the ability of partial recovery of the signal loss caused by ferromagnetic objects in the field of view [72]. Therefore, images acquired by spin-echo based sequences are expected to attain much better characteristics than those acquired by gradient-echo based sequences. Present findings are in good agreement with this expectation and underline a major concern in designing a prostate biopsy procedure under MRI.

As a conclusion of the prostate biopsy needle gun trial results, the conventional prostate biopsy needle gun is the most efficient compared to other two needles due to the biopsy sample weights that are taken from fresh veal meat. Although the expectations, spiral prostate biopsy needle handle was not so efficient because of insufficient rotational speed, and also the outer needle cannot cut the tissue effectively due to jamming of the tissue between outer and inner needle. Nevertheless, using nitinol wire instead of nitinol rod increased the cutting performance and efficiency of needle with collecting more tissue. Finally, new handle designs with different penetration mechanisms increased the efficiency of the prostate biopsy needle biopsy.

4.1 Conclusion

Overcoming technical challenges associated with the presence of a high magnetic field and preserving image quality, we have developed an MRI visible prostate biopsy needle that enables real-time passive device tracking. Furthermore, two MRI compatible biopsy guns have been designed to shot needles with different propelling profiles. Although prostate is the only organ that allows for a standardized biopsy sampling routines given its small surface area, targeting biopsy regions is highly desirable to ease interventional procedures and to reduce patient discomfort without sacrificing diagnostic accuracy. Besides its exclusive benefits in decreasing under diagnosis and false positive reports of PCa in clinical imaging, MRI is a highly promising method for targeting biopsy regions. Therefore, utilization of this biopsy needle, which is specifically tailored for MRI, holds considerable implications in clinical practice like causing less bleeding, decreasing infection risk and number of biopsy sample that are redundant because of imaging the exact tumor location with MRI. All these advantages shorten the biopsy session time that traumatize the patient with less pain.

4.2 Limitations of the Study

Usage of Fe_2O_3 coatings constitutes a major limitation since they do not hold on nitinol material perfectly and its ferromagnetic characteristic is not preferable for MRI. In order to overcome this limitation, alternative nanoparticles that can be coated onto the needles will be searched and tried. But also a cover method will be searched to decrease the toxic effect of the iron oxide and ferromagnetic characteristic [73, 74].

Another limitation of the study is related to nitinol elasticity. Because of the elasticity of the nitinol, the needle cannot be successful on penetration to extracapsular regions and providing an efficient sample. To overcome this problem, needles with MRI compatible and higher mechanical strength should be improved. Furthermore, laser cutting process for nitinol needle fabrication is a hard process because nitinol needle is

exposed to a thermal process which makes nitinol needles fragile. Since we are using nitinol wire instead of nitinol rod, the fragility of nitinol needle is getting higher. This is why we need to prefer nitinol needle with a thicker wall, but at the end, this thicker wall property makes laser cutting process difficult, and we observed fractions during cutting process [75].

Limitations are not only related to the product but also present in the testing processes. We did not test our product on a real prostatic tissue. The tissue that we used in our in vitro experiments is different than the original prostatic tissue. We did not test our device in vivo and get samples under the MRI. However, the primary purpose of this study is designing and fabrication of a novel biopsy needle instead of revealing comprehensive testing.

4.3 Prospective Studies

An important question for the future studies is how to improve the needle and handle designs to further increase efficiency of the biopsy procedure. First off, the needle diameter is planning to be decreased for less pain of puncture while preserving the durableness and tissue removal success. Designing a new configuration with different puncturing angle and tip designs can also ease the needles sinking into the tissue and tissue removal and makes the biopsy session painless. An additional improvement on the design would be closing the tip of the needle, which is left open by default due to nitinol wire. This modification may provide a more efficient penetration and sampling.

Iron oxide nanoparticles that are mixed with UV cure solution are coated with a fine brush onto the needle, but later in the project, sputtering will be used for iron oxide coating to increase the adhesion and regularity.

The final prostate biopsy system prototype was evaluated by using fresh veal meat. For a next step of the project, interventional prostate biopsy training phantom (Figure 4.1) is planning to be used for in vitro testing.
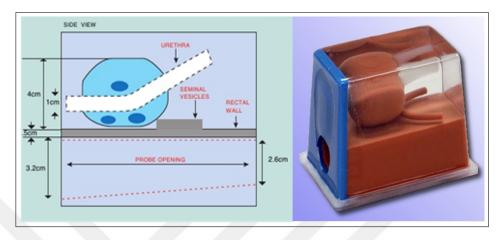
Figure 4.1 MRI visible tissue equivalent prostate phantom.

The prostate biopsy phantom will be imaged using TSE sequence and the lesion will be marked with virtual marker. Next, accession planes of tumor lesions will be detected. The biopsy robot will follow the directions and will be fixed. T2 weighted MR sequences will be used to obtain an image of biopsy needle markers, and real time MR sequences will be used to determine the orientation of biopsy robot and the needle will move across the phantom. During the needle insertion, the sensor will measure and record the force changes between normal tissue and a cancerous cell. Moreover, MR contrast solution will be injected (1:20 dilution) before the needle removing and 3D volumetric MR images will be obtained to determine probable axial, coronal, sagittal deviations between target location and biopsy robot tip location.

Stainless steel springs has been used to test the prostate biopsy handle shooting mechanism. To further increase MRI compatibility of the design, a nitinol spring to shoot needle is planned to be produced in the laboratory.

Moreover, without sacrificing MRI compatibility, design parameters can be improved to achieve a higher mechanical strength, which eventually would yield a more efficient sampling, especially for the regions attaining a hard surface. Lastly, alternative nanoparticles can be coated onto the needles with more robust coating methods

those enable a stronger grip of the MRI visible distance markers.

Second part of project is developing an MRI guided robot-assisted prostate biopsy to achieve an easier and a more precise targeting. This robot will be equipped with the needle and handle that are designed and produced in this work. Such combination with robotic assistance is highly promising to bring MRI guided targeted prostate biopsy one more step closer to the clinical practice.

REFERENCES

1. Heidenreich, A., J. Bellmunt, M. Bolla, S. Joniau, M. Mason, V. Matveev, N. Mottet, H.-P. Schmid, T. van der Kwast, T. Wiegel, *et al.*, "Eau guidelines on prostate cancer. part 1: screening, diagnosis, and treatment of clinically localised disease," *European urology*, Vol. 59, no. 1, pp. 61–71, 2011.

2. Stamey, T. A., J. E. McNeal, C. M. Yemoto, B. M. Sigal, and I. M. Johnstone, "Biological determinants of cancer progression in men with prostate cancer," *Jama*, Vol. 281, no. 15, pp. 1395–1400, 1999.

3. Yu, K. K., H. Hricak, R. Alagappan, D. M. Chernoff, P. Bacchetti, and C. J. Zaloudek, "Detection of extracapsular extension of prostate carcinoma with endorectal and phased-array coil mr imaging: multivariate feature analysis.," *Radiology*, Vol. 202, no. 3, pp. 697–702, 1997.

4. Weinreb, J. C., J. O. Barentsz, P. L. Choyke, F. Cornud, M. A. Haider, K. J. Macura, D. Margolis, M. D. Schnall, F. Shtern, C. M. Tempany, *et al.*, "Pi-rads prostate imaging–reporting and data system: 2015, version 2," *European urology*, Vol. 69, no. 1, pp. 16–40, 2016.

5. Moore, C. M., N. L. Robertson, N. Arsanious, T. Middleton, A. Villers, L. Klotz, S. S. Taneja, and M. Emberton, "Image-guided prostate biopsy using magnetic resonance imaging–derived targets: a systematic review," *European urology*, Vol. 63, no. 1, pp. 125–140, 2013.

6. Yuen, J., C. Thng, P. Tan, L. Khin, S. Phee, D. Xiao, W. Lau, W. Ng, and C. Cheng, "Endorectal magnetic resonance imaging and spectroscopy for the detection of tumor foci in men with prior negative transrectal ultrasound prostate biopsy," *The Journal of urology*, Vol. 171, no. 4, pp. 1482–1486, 2004.

7. Fiset, P. O., A. Aprikian, and F. Brimo, "Length of prostate biopsy cores: does it impact cancer detection," *Can J Urol*, Vol. 20, no. 4, pp. 6848–6853, 2013.

8. Öbek, C., T. Doğanca, S. Erdal, S. Erdoğan, and H. Durak, "Core length in prostate biopsy: size matters," *The Journal of urology*, Vol. 187, no. 6, pp. 2051–2055, 2012.

9. Daum, W., and A. Winkel, "Method and apparatus for mr-guided biopsy," Feb. 14 2003. US Patent App. 10/366,831.

10. Duerig, T., A. Pelton, and D. Stöckel, "An overview of nitinol medical applications," *Materials Science and Engineering: A*, Vol. 273, pp. 149–160, 1999.

11. Hricak, H., G. Dooms, J. E. McNeal, A. S. Mark, M. Marotti, A. Avallone, M. Pelzer, E. C. Proctor, and E. A. Tanagho, "Mr imaging of the prostate gland: normal anatomy," *American journal of roentgenology*, Vol. 148, no. 1, pp. 51–58, 1987.

12. Ellis, H., "Anatomy of the urinary bladder, prostate and male urethra," *Surgery (Oxford)*, Vol. 23, no. 3, pp. 97–98, 2005.

13. Lee, C. H., O. Akin-Olugbade, and A. Kirschenbaum, "Overview of prostate anatomy, histology, and pathology," *Endocrinology and metabolism clinics of North America*, Vol. 40, no. 3, pp. 565–575, 2011.

14. Coakley, F. V., and H. Hricak, "Radiologic anatomy of the prostate gland: a clinical approach," *Radiologic Clinics of North America*, Vol. 38, no. 1, pp. 15–30, 2000.

15. "SEER Training Modules." `https://training.seer.cancer.gov/prostate/anatomy`, 2003. Retrieved 20 May 2017.

16. Hammerich, K. H., G. E. Ayala, and T. M. Wheeler, "Anatomy of the prostate gland and surgical pathology of prostate cancer," *Cambridge University, Cambridge*, pp. 1–10, 2009.

17. "American college of radiology and reporting, mr prostate imaging, data system version 2.0." `https://www.acr.org/Quality-Safety/Resources/PIRADS`, 2015. Retrieved 25 May 2017.

18. Cohen, R. J., B. A. Shannon, M. Phillips, R. E. Moorin, T. M. Wheeler, and K. L. Garrett, "Central zone carcinoma of the prostate gland: a distinct tumor type with poor prognostic features," *The Journal of urology*, Vol. 179, no. 5, pp. 1762–1767, 2008.

19. McNeal, J. E., "The zonal anatomy of the prostate," *The prostate*, Vol. 2, no. 1, pp. 35–49, 1981.

20. Schröder, F. H., J. Hugosson, M. J. Roobol, T. L. Tammela, S. Ciatto, V. Nelen, M. Kwiatkowski, M. Lujan, H. Lilja, M. Zappa, *et al.*, "Screening and prostate-cancer mortality in a randomized european study," *N Engl j Med*, Vol. 2009, no. 360, pp. 1320–1328, 2009.

21. Presti Jr, J. C., "Prostate biopsy: current status and limitations," *Reviews in urology*, Vol. 9, no. 3, p. 93, 2007.

22. Catalona, W. J., D. S. Smith, R. L. Wolfert, T. J. Wang, H. G. Rittenhouse, T. L. Ratliff, and R. B. Nadler, "Evaluation of percentage of free serum prostate-specific antigen to improve specificity of prostate cancer screening," *Jama*, Vol. 274, no. 15, pp. 1214–1220, 1995.

23. Yeo, L., A. Papatsoris, C. Bach, D. Patel, I. Junaid, J. Masood, and N. Buchholz, *The development of the modern prostate biopsy*, INTECH Open Access Publisher, 2011.

24. Bjurlin, M. A., J. S. Wysock, and S. S. Taneja, "Optimization of prostate biopsy: review of technique and complications," *Urologic Clinics of North America*, Vol. 41, no. 2, pp. 299–313, 2014.

25. Bales, G., T. Flynn, H. Kynaston, A. Golash, A. Hart, H. Kim, and G. Gerber, "Role of transurethral biopsy sampling of the prostate to diagnose prostate cancer in men undergoing surgical intervention for benign prostatic hyperplasia.," *Techniques in urology*, Vol. 6, no. 3, pp. 201–204, 2000.

26. Rovner, E. S., F. J. Schanne, B. Malkowicz, and A. J. Wein, "Transurethral biopsy of the prostate for persistently elevated or increasing prostate specific antigen following multiple negative transrectal biopsies," *The Journal of urology*, Vol. 158, no. 1, pp. 138–142, 1997.

27. Franzen, S., G. Giertz, and J. Zajicek, "Cytological diagnosis of prostatic tumours by transrectal aspiration biopsy: a preliminary report," *BJU International*, Vol. 32, no. 2, pp. 193–196, 1960.

28. Adhyam, M., and A. K. Gupta, "A review on the clinical utility of psa in cancer prostate," *Indian journal of surgical oncology*, Vol. 3, no. 2, pp. 120–129, 2012.

29. Partin, A. W., W. J. Catalona, P. C. Southwick, E. N. Subong, G. H. Gasior, and D. W. Chan, "Analysis of percent free prostate-specific antigen (psa) for prostate cancer detection: influence of total psa, prostate volume, and age," *Urology*, Vol. 48, no. 6, pp. 55–61, 1996.

30. Hodge, K., J. McNeal, and T. Stamey, "Ultrasound guided transrectal core biopsies of the palpably abnormal prostate.," *The Journal of urology*, Vol. 142, no. 1, pp. 66–70, 1989.

31. Purohit, R. S., K. Shinohara, M. V. Meng, and P. R. Carroll, "Imaging clinically localized prostate cancer," *Urologic Clinics of North America*, Vol. 30, no. 2, pp. 279–293, 2003.

32. McCormack, M., A. Duclos, M. Latour, M. H. McCormack, D. Liberman, O. Djahangirian, J. Bergeron, L. Valiquette, and K. Zorn, "Effect of needle size on cancer detection, pain, bleeding and infection in trus-guided prostate biopsies: a prospective trial," *Canadian Urological Association Journal*, Vol. 6, no. 2, p. 97, 2012.

33. Bhavsar, A., and S. Verma, "Anatomic imaging of the prostate," *BioMed research international*, Vol. 2014, 2014.

34. Karakiewicz, P. I., M. Bazinet, A. G. Aprikian, C. Trudel, S. Aronson, M. Nachabé, F. Péloquint, J. Dessureault, M. S. Goyal, L. R. Bégin, *et al.*, "Outcome of sextant biopsy according to gland volume," *Urology*, Vol. 49, no. 1, pp. 55–59, 1997.

35. "Mayo Clinic Prostate Biopsy, What you can expect?." `http://www.mayoclinic.org/tests-procedures/prostate-biopsy/details/what-you-can-expect/rec-20200191`, 2008. Retrieved 3 June 2017.

36. Shinohara, K., P. Scardino, S. S. Carter, and T. Wheeler, "Pathologic basis of the sonographic appearance of the normal and malignant prostate.," *The Urologic clinics of North America*, Vol. 16, no. 4, pp. 675–691, 1989.

37. Shinohara, K., T. M. Wheeler, and P. T. Scardino, "The appearance of prostate cancer on transrectal ultrasonography: correlation of imaging and pathological examinations.," *The Journal of urology*, Vol. 142, no. 1, pp. 76–82, 1989.

38. Trabulsi, E. J., D. Sackett, L. G. Gomella, and E. J. Halpern, "Enhanced transrectal ultrasound modalities in the diagnosis of prostate cancer," *Urology*, Vol. 76, no. 5, pp. 1025–1033, 2010.

39. Brenner, D. J., "Should we be concerned about the rapid increase in ct usage?," *Reviews on environmental health*, Vol. 25, no. 1, p. 63, 2010.

40. Webb, A., *Introduction to biomedical imaging*, Wiley-Interscience, 2003.

41. Husarik, D. B., R. Miralbell, M. Dubs, H. John, O. T. Giger, A. Gelet, T. Cservenyàk, and T. F. Hany, "Evaluation of [18f]-choline pet/ct for staging and restaging of prostate cancer," *European journal of nuclear medicine and molecular imaging*, Vol. 35, no. 2, pp. 253–263, 2008.

42. Farsad, M., R. Schiavina, P. Castellucci, C. Nanni, B. Corti, G. Martorana, R. Canini, W. Grigioni, S. Boschi, M. Marengo, *et al.*, "Detection and localization of prostate cancer: correlation of 11c-choline pet/ct with histopathologic step-section analysis," *Journal of Nuclear Medicine*, Vol. 46, no. 10, pp. 1642–1649, 2005.

43. Haas, G. P., and W. A. Sakr, "Epidemiology of prostate cancer," *CA: a cancer journal for clinicians*, Vol. 47, no. 5, pp. 273–287, 1997.

44. Turkbey, B., M. J. Merino, E. C. Gallardo, V. Shah, O. Aras, M. Bernardo, E. Mena, D. Daar, A. R. Rastinehad, W. M. Linehan, *et al.*, "Comparison of endorectal coil and nonendorectal coil t2w and diffusion-weighted mri at 3 tesla for localizing prostate cancer: Correlation with whole-mount histopathology," *Journal of Magnetic Resonance Imaging*, Vol. 39, no. 6, pp. 1443–1448, 2014.

45. Steinseifer, I. K., J. J. van Asten, E. Weiland, T. W. Scheenen, M. C. Maas, and A. Heerschap, "Improved volume selective 1h mr spectroscopic imaging of the prostate with gradient offset independent adiabaticity pulses at 3 tesla," *Magnetic resonance in medicine*, Vol. 74, no. 4, pp. 915–924, 2015.

46. Hegde, J. V., R. V. Mulkern, L. P. Panych, F. M. Fennessy, A. Fedorov, S. E. Maier, and C. Tempany, "Multiparametric mri of prostate cancer: An update on state-of-the-art techniques and their performance in detecting and localizing prostate cancer," *Journal of Magnetic Resonance Imaging*, Vol. 37, no. 5, pp. 1035–1054, 2013.

47. Miao, H., H. Fukatsu, and T. Ishigaki, "Prostate cancer detection with 3-t mri: comparison of diffusion-weighted and t2-weighted imaging," *European journal of radiology*, Vol. 61, no. 2, pp. 297–302, 2007.

48. Le Bihan, D., E. Breton, D. Lallemand, P. Grenier, E. Cabanis, and M. Laval-Jeantet, "Mr imaging of intravoxel incoherent motions: application to diffusion and perfusion in neurologic disorders.," *Radiology*, Vol. 161, no. 2, pp. 401–407, 1986.

49. Vargas, H. A., O. Akin, T. Franiel, Y. Mazaheri, J. Zheng, C. Moskowitz, K. Udo, J. Eastham, and H. Hricak, "Diffusion-weighted endorectal mr imaging at 3 t for prostate cancer: tumor detection and assessment of aggressiveness," *Radiology*, Vol. 259, no. 3, pp. 775–784, 2011.

50. Basser, P. J., J. Mattiello, and D. LeBihan, "Estimation of the effective self-diffusion tensor from the nmr spin echo," *Journal of Magnetic Resonance, Series B*, Vol. 103, no. 3, pp. 247–254, 1994.

51. Pierpaoli, C., and P. J. Basser, "Toward a quantitative assessment of diffusion anisotropy," *Magnetic resonance in Medicine*, Vol. 36, no. 6, pp. 893–906, 1996.

52. Hosseinzadeh, K., and S. D. Schwarz, "Endorectal diffusion-weighted imaging in prostate cancer to differentiate malignant and benign peripheral zone tissue," *Journal of Magnetic Resonance Imaging*, Vol. 20, no. 4, pp. 654–661, 2004.

53. Hittmair, K., G. Gomiscek, K. Langenberger, M. Recht, H. Imhof, and J. Kramer, "Method for the quantitative assessment of contrast agent uptake in dynamic contrast-enhanced mri," *Magnetic resonance in medicine*, Vol. 31, no. 5, pp. 567–571, 1994.

54. Hansford, B. G., Y. Peng, Y. Jiang, M. W. Vannier, T. Antic, S. Thomas, S. McCann, and A. Oto, "Dynamic contrast-enhanced mr imaging curve-type analysis: is it helpful in the differentiation of prostate cancer from healthy peripheral zone?," *Radiology*, Vol. 275, no. 2, pp. 448–457, 2015.

55. Banaś, K., A. Jasiński, A. M. Banaś, M. Gajda, G. Dyduch, B. Pawlicki, and W. M. Kwiatek, "Application of linear discriminant analysis in prostate cancer research by synchrotron radiation-induced x-ray emission," *Analytical chemistry*, Vol. 79, no. 17, pp. 6670–6674, 2007.

56. Thompson, J., N. Lawrentschuk, M. Frydenberg, L. Thompson, and P. Stricker, "The role of magnetic resonance imaging in the diagnosis and management of prostate cancer," *BJU international*, Vol. 112, no. S2, pp. 6–20, 2013.

57. Villeirs, G. M., K. L. Verstraete, W. J. De Neve, and G. O. De Meerleer, "Magnetic resonance imaging anatomy of the prostate and periprostatic area: a guide for radiotherapists," *Radiotherapy and Oncology*, Vol. 76, no. 1, pp. 99–106, 2005.

58. Kim, C. K., "Magnetic resonance imaging-guided prostate biopsy: present and future," *Korean journal of radiology*, Vol. 16, no. 1, pp. 90–98, 2015.

59. Nagarajappa, N., "Background suppression using hadamard rf pulses for endovascular therapy in magnetic resonance," 2004.

60. Unal, O., F. R. Korosec, R. Frayne, C. M. Strother, and C. A. Mistretta, "A rapid 2d time-resolved variable-rate k-space sampling mr technique for passive catheter tracking during endovascular procedures," *Magnetic resonance in medicine*, Vol. 40, no. 3, pp. 356–362, 1998.

61. Wang, Y., P. J. Rossman, R. C. Grimm, A. H. Wilman, S. J. Riederer, and R. L. Ehman, "3d mr angiography of pulmonary arteries using realtime navigator gating and magnetization preparation," *Magnetic resonance in medicine*, Vol. 36, no. 4, pp. 579–587, 1996.

62. Dixon, W. T., L. N. Du, D. D. Faul, M. Gado, and S. Rossnick, "Projection angiograms of blood labeled by adiabatic fast passage," *Magnetic resonance in medicine*, Vol. 3, no. 3, pp. 454–462, 1986.

63. Draper, J. N., M. L. Lauzon, and R. Frayne, "Passive catheter visualization in magnetic resonance–guided endovascular therapy using multicycle projection dephasers," *Journal of Magnetic Resonance Imaging*, Vol. 24, no. 1, pp. 160–167, 2006.

64. Abolhassani, N., R. Patel, and M. Moallem, "Needle insertion into soft tissue: A survey," *Medical engineering & physics*, Vol. 29, no. 4, pp. 413–431, 2007.

65. O'Leary, M. D., C. Simone, T. Washio, K. Yoshinaka, and A. M. Okamura, "Robotic needle insertion: Effects of friction and needle geometry," in *Robotics and Automation, 2003. Proceedings. ICRA'03. IEEE International Conference on*, Vol. 2, pp. 1774–1780, IEEE, 2003.

66. Ehmann, K., and K. Malukhin, "A generalized analytical model of the cutting angles of a biopsy needle tip," *Journal of Manufacturing Science and Engineering*, Vol. 134, no. 6, p. 061001, 2012.

67. Petrini, L., and F. Migliavacca, "Biomedical applications of shape memory alloys," *Journal of Metallurgy*, Vol. 2011, 2011.

68. "Comconic micro-blasting scheme." `http://www.comcoinc.com/microblaster`, 2012. Retrieved 2 June 2017.

69. Geraldes, C. F., and S. Laurent, "Classification and basic properties of contrast agents for magnetic resonance imaging," *Contrast media & molecular imaging*, Vol. 4, no. 1, pp. 1–23, 2009.

70. Bachman, J., "Torquing of stainless steel and nitinol wires: A comparison of mechanical properties," *Europ J Orthod*, Vol. 5, pp. 167–169, 1983.

71. Harris, C. A., and L. M. White, "Metal artifact reduction in musculoskeletal magnetic resonance imaging," *Orthopedic Clinics of North America*, Vol. 37, no. 3, pp. 349–359, 2006.

72. Wortmann, T., C. Dahmen, and S. Fatikow, "Study of mri susceptibility artifacts for nanomedical applications," *Journal of Nanotechnology in Engineering and Medicine*, Vol. 1, no. 4, p. 041002, 2010.

73. Teja, A. S., and P.-Y. Koh, "Synthesis, properties, and applications of magnetic iron oxide nanoparticles," *Progress in crystal growth and characterization of materials*, Vol. 55, no. 1, pp. 22–45, 2009.

74. Pisanic, T. R., J. D. Blackwell, V. I. Shubayev, R. R. Fiñones, and S. Jin, "Nanotoxicity of iron oxide nanoparticle internalization in growing neurons," *Biomaterials*, Vol. 28, no. 16, pp. 2572–2581, 2007.

75. Guo, Y., A. Klink, C. Fu, and J. Snyder, "Machinability and surface integrity of nitinol shape memory alloy," *CIRP Annals-Manufacturing Technology*, Vol. 62, no. 1, pp. 83–86, 2013.